# Selective separation of manganese, cobalt and nickel in a fully aqueous system

Nicolas Schaeffer,[a] Helena Passos,[a] Matthieu Gras,[b] Sílvia Juliana Rodriguez Vargas,[a] Márcia C. Neves,[a] Lenka Svecova,[b] Nicolas Papaiconomou[c] and João A.P. Coutinho*[a]

[a] *CICECO, Aveiro Institute of Materials, Department of Chemistry, University of Aveiro, Campus Universitário de Santiago, 3810-193 Aveiro, Portugal.*

[b] *Univ. Grenoble Alpes, Univ. Savoie Mont Blanc, CNRS, Grenoble INP, LEPMI, 38000 Grenoble, France.*

[c] *Université Nice Sophia Antipolis, Department of Chemistry, 28 Avenue Valrose, 06103 Nice, France*

* Corresponding authors: jcoutinho@ua.pt

## Abstract

The continued electrification of society and the related growing demand for rechargeable batteries requires in turn the elaboration of efficient and sustainable recycling strategies for their recovery and valorization. An important separation relevant to Nickel Metal Hydride (NiMH) and Lithium-Ion battery recycling is the inter-transition elements separation between Ni(II), Co(II), and Mn(II). In this work, a fully aqueous process for the recovery of Mn(II) and Co(II) from concentrated Ni(II) effluents typical of NiMH battery leachate is disclosed consuming only $Na_2CO_3$. In the first instance, Mn is selectively precipitated as Mn(IV) by oxidation using ozone as oxidant, resulting in a significant enrichment of Mn in the precipitate relative to its original solution concentration. Secondly, the thermo- and acid-responsive aqueous biphasic system (ABS) based on the ionic liquid (IL) tributyltetradecylphosphonium chloride ($[P_{44414}]Cl$) and $NiCl_2$ was used to recover Co(II). By using the high $NiCl_2$ content found in NiMH leachates both as ABS phase former and salting-out agent, no additional salt is required. Through careful manipulation of the Co(II) to Ni(II) and the IL to Co(II) molar ratios, an effective and selective separation of Co(II) from Ni(II) was achieved. Finally, Co(II) is precipitated from the IL-rich phase and the IL is regenerated in one step by addition of $Na_2CO_3$ to induce a new phase separation.

**Keywords**: aqueous biphasic system, battery recycling, cobalt, metal separation, selective precipitation

# Introduction

At the forefront of climate change mitigation measures is the switch to electricity derived from renewable energy and the electrification of the transport sector, their implementation being heavily reliant on rechargeable battery technology. The demand for batteries is further compounded by the increasing digitalization of consumer goods.[1] It is estimated that approximately 800,000 tons of automotive batteries, 190,000 tons of industrial batteries, and 160,000 tons of consumer batteries enter the European Union each year alone, with global demand forecasted to grow significantly over the next five years.[1,2] This increasing consumption in turn yields a corresponding waste generation which needs to be adequately addressed both to valorise the economic value of the critical raw materials present within whilst mitigating the environmental impact of the waste. End-of-life battery recycling is an area of active research due to the inherent material value and potential toxicity of the waste, with the various options including pyrometallurgy, hydrometallurgy or direct recycling detailed in recent reviews.[1,3,4]

One of the most critical inter-element separations facing the recycling of Nickel Metal Hydride (NiMH) and Lithium-ion batteries (LIBs) is the separation of transition metals nickel, cobalt, and manganese. The price and concerns surrounding cobalt production results in its gradual substitution in LIB cathodes and the increasing market share of $LiNi_xCo_yMn_zO_2$ chemistry[3] whilst NiMH batteries with $AB_5$-type anodes represent a rich secondary source for these elements.[4,5] Amongst the variety of reported hydrometallurgical separation systems, selected ionic liquids (ILs) demonstrated an excellent ability to separate Co(II) and Ni(II).[6-11] These ILs typically incorporating a chloride anion exploit the difference in complexation constants of Ni(II) and Co(II) with chloride ($k_1(NiCl^+)=0.07$ whilst $k_4(CoCl_4^{2-})=2.77$)[12] to extract the resulting neutral or anionic chlorocobalt complex via an ion-pairing or anion-exchange mechanism.[13] Problematically, Mn(II) is partly co-extracted with Co(II) as it too forms chloro complexes, requiring additional purification steps.[6-11] Furthermore, the application of chloride-based hydrophobic ILs remains hampered by their high viscosities, especially once loaded with metals, due to the long cationic alkyl moieties required to confer sufficient hydrophobicity.

This work presents a study detailing the entirely aqueous separation of Mn(II) and Co(II) from concentrated Ni(II) solution through the exploration of the different intrinsic properties of these metals. Firstly, the selective recovery of Mn(II) from a mixed metal solution is assessed by taking advantage of the Mn(II) ↔ Mn(IV) redox pair and the low solubility of $MnO_2$. Secondly, the difference in chloride complexation between Co(II) and Ni(II) is applied towards the extraction of Co(II) in an IL-based aqueous biphasic system (ABS) directly using the high Ni(II) concentration to induce the ABS creation and to salt-out Co(II) selectively. To this end, the ABS composed of the IL tributyltetradecylphosphonium chloride ($[P_{44414}]Cl$) is employed due to its responsiveness to acid and temperature conditions, allowing for a fine-tuning of Co(II) extraction by the adjustment of several parameters.[11,14-17] Finally, the extracted Co(II) is precipitated and the IL regenerated in one single step.

A schematic of the process followed in this work is presented in **Figure 1**. Conducting the entire process in aqueous media using smaller quantities of ILs mitigates the typical limitations of these solvents, namely their high viscosity and cost, whilst retaining their proven advantageous properties.

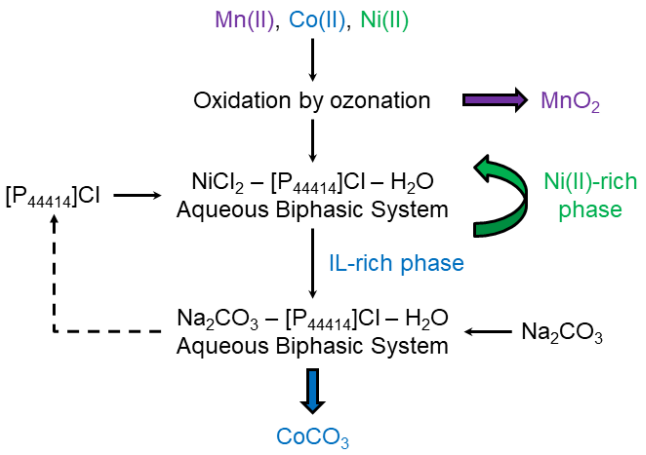


**Figure 1.** Schematic of the process outlined in this work for the aqueous separation of Mn(II), Co(II) and Ni(II).

## Methodology

A detailed description of the materials and methods used in this work is described in the Supplementary Information (SI). Tributyltetradecyl phosphonium chloride ($[P_{44414}]Cl$) was purchased from Iolitec in 95.0 wt.% purity and confirmed as 97.1 wt.% pure by quantitative $^{1}$H-NMR analysis. $[P_{44414}]Cl$ is a waxy solid with a melting point of 38.5 $^{o}$C [14] and is fully soluble in water for all IL concentrations. The aqueous phase behaviour of $[P_{44414}]Cl$ alone and in the presence of common salts and inorganic acids was previously reported, with aqueous solution of $[P_{44414}]Cl$ presenting an intriguing upper critical solution temperature behaviour typically associated with non-ionic surfactants.[16,17]

### Oxidation of Mn(II) to Mn(IV) by ozonation

A commercially available domestic ozone generator (Lufthous$O_3$ from Lufthous) was used in all experiments delivering a fixed gas flow rate of 1.0 L.min$^{-1}$ monitored and a consistent ozone flow rate of 0.768 g.hr$^{-1}$ (0.016 mol.hr$^{-1}$). The ozone flow rate was determined by colorimetric titration using potassium iodide and sodium thiosulfate ($Na_2S_2O_3$), with the calibration procedure described in the SI. Mn(II) precipitation was monitored as a function of the solution acid concentration (0.0 and 3.7 wt.% HCl) and time. A constant solution composition with a Mn:Co:Ni molar ratio of 0.07:0.17:1.00

containing 0.023, 0.054 and 0.320 mol.kg$^{-1}$ of Mn, Co and Ni respectively, was used. The kinetic of Mn(II) oxidation were determined by collecting 1 mL aliquot at specific time intervals over a 8 hr period of continuous ozonation and the solution analysed by atomic adsorption spectroscopy (AAS) after appropriate dilution. The precipitation yield of manganese was calculated by mass balance after AAS analysis of the aqueous ozonated solution according to equation (1).

$$Yield_{Mn(IV)} = \frac{([Mn]_{in} - [Mn]_f)}{[Mn]_{in}} \times 100 \quad \text{- (1)}$$

where the subscripts *in* denotes the solution before ozonation and *f* the aqueous phase after ozonation for a given time t (min). The precipitate obtained at the end of the ozonation period was recovered by filtration, rinsed with deionized water and analysed by scanning electron microscopy (SEM) with energy-dispersive X-ray spectroscopy (EDS) and AAS after dissolution in 4 mol.L$^{-1}$ HCl.

**Determination of $MCl_2$-[$P_{44414}$]Cl-$H_2O$ phase diagram and cobalt speciation with temperature**

The procedure followed in this work for the experimental determination of binodal curves for ternary and quaternary systems was previously reported and is detailed in the SI.[18] The temperature dependency of phase-separation in the $MCl_2.6H_2O$–[$P_{44414}$]Cl–$H_2O$ ternary systems for a fixed composition, where M is either cobalt or nickel, was assessed using the cloud point method, i.e. the temperature at which the solution becomes turbid indicating phase demixing. A constant [$P_{44414}$]Cl concentration of 0.46 mol.kg$^{-1}$ (20 wt.%) was used throughout and the $MCl_2$ concentration varied from 0.00 to 0.63 mol.kg$^{-1}$. The ternary system compositions were determined by the weight quantification of all components added within an uncertainty of $\pm 10^{-3}$ g. Two replicates were taken for each composition with an error of less than 1.0 °C. The systems were heated between 10.0 °C and 98.0 °C with a heating rate of 0.5 °C.min$^{-1}$ in a temperature-controlled water bath with a precision of ±0.01 °C (ME-18 V Visco-Thermostat, Julabo). For the system composed of [$CoCl_2.6H_2O$] = 0.52 mol.kg$^{-1}$ and [$P_{44414}$]Cl = 0.46 mol.kg$^{-1}$, the temperature induced change in cobalt speciation and micellar phase transition of the [$P_{44414}$]Cl surfactant was followed by dynamic light scattering (DLS) and UV-vis in the range from 10.0 °C to 34.0 °C at regular temperature intervals. All measurements were performed using ultrapure water and left to equilibrate at the desired temperature for 30 min prior to measurements. Each temperature condition was analysed three separate times over a 2 hr period to ensure the formation of stable aggregates.

**Cobalt/Nickel separation, cobalt recovery and [$P_{44414}$]Cl regeneration**

The partition behavior of cobalt and nickel in the $NiCl_2$–[$P_{44414}$]Cl–$H_2O$ ABS at 50.0 °C and composed of 20 wt.% [$P_{44414}$]Cl was studied as a function the cobalt to nickel molar ratio ($\chi_{Co}$) ranging from 0.00 to 0.33

and calculated as follows.

$$x_{Co} = \frac{n_{Co}}{n_{Co}+n_{Ni}} \quad \text{-(2)}$$

Three different extraction systems were studied based on the total chloride concentration, namely (i) [$NiCl_2.6H_2O$]=0.35 mol.kg$^{-1}$, (ii) [$NiCl_2.6H_2O$]=0.35 mol.kg$^{-1}$ supplemented with 3.7 wt.% HCl, and (iii) [$NiCl_2.6H_2O$]=1.00 mol.kg$^{-1}$. The total system mass is of 5 g. Typically, 4 g of an initial aqueous solution containing the desired concentration of $CoCl_2.6H_2O$, $NiCl_2.6H_2O$ and HCl is mixed with 1 g IL. The solution is mechanically agitated until the complete dissolution of the IL. The resulting mixture is left to phase separate 2 hrs in a thermostatic bath at 50.0 $^{o}$C. The volume of each phase of the ABS is recorded and aliquots of the upper and lower phases are collected for metal concentration analysis by AAS after appropriate dilution. Metal ion ($M^{n+}$) distribution coefficients ($D_M$) and the separation factor between cobalt and nickel ($\alpha_{Co/Ni}$) are calculated using Equations (3) and (4) where the subscript *IL* and *aq* denote the respective phase.

$$D_M = [M^{n+}]_{IL} / [M^{n+}]_{aq} \quad \text{-(3)}$$

$$\alpha_{Co/Ni} = D_{Co} / D_{Ni} \quad \text{-(4)}$$

Following cobalt extraction under the determined optimal conditions (extraction conditions - $\chi_{Co}$ = 0.20 and [$NiCl_2.6H_2O$] = 1.00 mol.kg$^{-1}$), the IL-rich phase (top phase) was separated, isolated and diluted in a determined volume of deionised water. The recovery of cobalt from the IL-rich phase by $Na_2CO_3$ precipitation was followed as a function of the predominant cobalt complex in solution. After separation and isolation of IL-rich phase the latter was diluted either three times or 8 times, yielding a final blue or red solution, respectively. This well-known color change is due to the transition of anionic chlorocobalt complexes to red cobalt hexahydrate complex. To this solution, 1.25 times the stochiometric quantity of anhydrous $Na_2CO_3$ was added, based on AAS quantification of cobalt in the IL-rich phase and assuming a 1:1 $Co^{2+}$:$CO_3^{2-}$ ratio, and agitated for 5 min. The precipitate was recovered by centrifugation, rinsed with deionised water and dried at 50.0 $^{o}$C for 48 hrs before analysis by SEM-EDS. To the IL solution, $Na_2CO_3$ was further added to yield a final concentration of 10 wt.% and the system left to phase separate 1 hr in a thermostatic bath. The IL-rich phase is then recovered, analysed by Fourier transform infrared (FTIR) as well as $^{1}$H-,$^{12}$C- and $^{31}$P-NMR spectroscopy and compared to that of the original [$P_{44414}$]Cl.

# Results and Discussion

**Selective precipitation of manganese by ozonation**

Contrary to Ni(II) whose aqueous speciation is largely independent of chloride concentration (predominance of the $[NiCl(H_2O)_5]^+$ and $[Ni(H_2O)_6]^{2+}$ species),[19] Mn(II) can form a range of chloro-complexes, including neutral and anionic ones, with increasing chloride concentration and temperature.[20] The emergence of these complexes typically overlaps the chloride concentration range for maximal Co(II) extraction by basic extractants and renders their mutual separation in a single step challenging.[7-11,13,14] If achievable, selective precipitation represents one of the most industrially applicable approaches to metal recovery due to its simple process requirements and greatly simplifies downstream separations.[21] As such, the selective precipitation of Mn(II) from a solution containing Co(II) and Ni(II) was attempted by oxidation of Mn(II) to Mn(IV) and the subsequent precipitation of the very sparingly soluble $MnO_2$ specie.[22-25] Ozone ($O_3$) was selected as oxidising agent as (i) it can efficiently oxidise Mn(II) according to the potential-pH diagram of the Mn-$H_2O$ system (reactions 5-7),[24,25] (ii) it is generated and consumed *in-situ*, minimising the need for storage and (iii) does not introduce potential metal impurities into the solution unlike metal oxidants such as ferrate (Fe(VI)).

$$O_3 + 2H^+ + 2e^- \rightleftharpoons O_2 + H_2O, \qquad E^0 = 2.076\ V\ ^{26} \qquad -(5)$$

$$MnO_2(s) + 4H^+ + 2e^- \rightleftharpoons Mn^{2+} + 2H_2O, \quad E^0 = 1.240\ V\ ^{23} \qquad -(6)$$

$$3Mn^{2+}(aq) + O_3(g) + 3H_2O(aq) \rightarrow 3MnO_2(s) + 6H^+(aq) \qquad -(7)$$

where $E^0$ is the standard electrode potential (V). A starting solution with a Mn:Co:Ni molar ratio of 0.07:0.17:1.00 typical of NiMH battery leachate[5] ($[NiCl_2.6H_2O]$=0.32 mol.kg$^{-1}$) was used and the precipitation yield assessed as a function of the solution acid concentration (0.0 and 1.0 mol.kg$^{-1}$ HCl, corresponding to 3.7 wt.% HCl) and time. Based on the ozone generator's calculated flow rate of $2.67\times10^{-6}$ mol.min$^{-1}$ $O_3$, an initial Mn(II) content of $3.37\times10^{-3}$ mol and a 1:3 $O_3$:$Mn^{2+}$ reaction stoichiometry, 420 min are theoretically required for complete Mn(II) precipitation. Under these conditions, the concentration of dissolved Mn(II) concentration with respect to time and HCl concentration, along with the resulting precipitation yield are presented in **Figure 2**. SEM-EDS analysis of the precipitate recovered after 480 min from a 3.7 wt.% HCl solution is also presented in **Figure 2.**

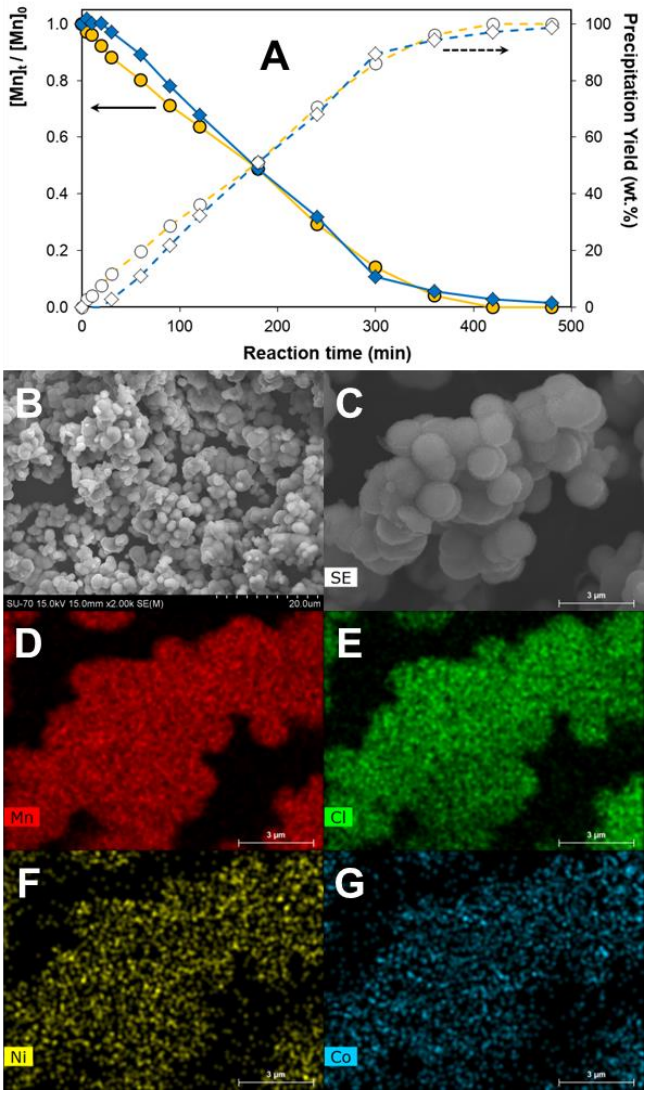


**Figure 2.** A) The influence of time and starting HCl concentration (yellow circle – 0.0 wt.% HCl, blue square – 3.7 wt.% HCl) on the Mn precipitation yield. A starting solution with a Mn:Co:Ni molar ratio of 0.07:0.17:1.00 ($[NiCl_2.6H_2O]$=0.32 mol.kg$^{-1}$) was used. B) SEM image; and EDS elemental mapping: C) SEM image, D)-G) the corresponding elemental mapping of Mn, Cl, Ni and Co, respectively of the precipitate recovered after 480 min from a 3.7 wt.% HCl solution.

Starting from an initial solution containing $[MnCl_2.4H_2O]$=0.023 mol.kg$^{-1}$, complete Mn precipitation is attained after 420 min in the $H_2O$ solution as predicted, with the concentration declining linearly until 300 min after which a decrease in the slope change is observed. Previous studies indicated that the kinetics of Mn oxidation are generally first order with respect to Mn and oxidant concentration during the initial stages of the reaction.[24-25] The final precipitation efficiency is largely unaffected by the initial solution acid concentration at the tested conditions, reaching a manganese precipitation yield of 97.3 % after 420 min for an initial HCl concentration of 3.7 wt.%. Importantly, the Co(II) and Ni(II)

concentrations during the precipitation process in both 0.0 and 3.7 wt.% HCl solutions remains constant with regards to their initial concentration within the experimental uncertainty (5.0%), **Figure S1 & S2** of the SI. Contrary to precipitation in neutral aqueous solution in which visible precipitation was instantly observed, more than 30 min are required for precipitation onset in 3.7 wt.% HCl solution. The increased acidity and chloride concentration of the 3.7 wt.% HCl solution could promote side reactions that delay the onset of Mn(IV) precipitation, such as the formation of permanganate or chlorine gas, Equation 8 and 9.

$$MnO_4^- + 8H^+ + 5e^- \rightleftharpoons Mn^{2+} + 4H_2O, \qquad E^0 = 1.510\ V\ ^{23} \qquad -(8)$$

$$Cl_2(g) + e^- \rightleftharpoons 2\ Cl^-(aq), \qquad E^0 = 1.396\ V \qquad -(9)$$

The redox potential of these side reactions is pH dependent and within the oxidation potential of ozone but greater than that of the Mn(II) to Mn(IV) pair (Equation 6), suggesting that whilst Mn(II) remains in solution the possibility of these side reactions is likely suppressed. UV-Vis analysis of the aqueous solution after 30 min did not indicate the presence of $MnO_4^-$. Furthermore, suspension of a litmus paper above the solution during ozonation did not result in its discoloration, indicating negligible chlorine gas formation. As such, the delay in $MnO_2$ precipitation in 3.7 wt.% HCl solution is tentatively attributed to the re-dissolution of the formed $MnO_2$ during the early stages.

SEM photographs of the obtained black powder after 480 min ozonation in $H_2O$ (**Figure S3**) and 3.7 wt.% HCl (**Figure 2**) show the presence of large aggregates composed of small spherical particles with a diameter of 1 to 5 µm. Compositional EDS analysis of the precipitates (**Figures S4 & S5**) summarized in **Table 1** identifies Mn as its primary metallic constituent. A significant chloride concentration is also present in both precipitates even after rinsing, as well as a greater Ni and Co contamination in the precipitate obtained in $H_2O$. It is proposed that the precipitation of $MnO_2$ acts as nucleation point for the local precipitation of Co and Ni chloride salts: the solution can be trapped within the pores of the precipitate and solubility can be locally overpassed. Despite the greater chloride concentration in 3.7 wt.% HCl, these deposits are subsequently re-leached resulting in lower impurity content relative to using $H_2O$ as media. Excluding chloride and oxygen, Mn represents 79.6 wt.% and 89.7 wt.% of the final precipitate obtained from pure $H_2O$ and 3.7 wt.% HCl aqueous solution, respectively. The starting solution containing 0.023, 0.054 and 0.320 $mol.kg^{-1}$ of Mn, Co and Ni, respectively, exhibited a Mn composition of 5.4 wt.%. Compared to this, the precipitates obtained in pure water and 3.7 wt.% HCl are thus enriched in Mn by a factor of 14.7 and 16.6, respectively. Unfortunately, characterisation of the precipitate by X-ray diffraction was prevented due to the important fluorescence of Co, Ni and Mn with the Cu source, yielding a diffractogram with a high noise to peak ratio. This makes it difficult to exclude the presence of other manganese oxide species beyond $MnO_2$, especially for precipitation under neutral pH conditions where the formation of $Mn_2O_3$ is possible. Overall, the oxidation-precipitation of Mn by ozonation appears as an efficient method for its aqueous recovery for a range of initial solution

acidity and even the presence of large excess of other metal salts. However, it is important to highlight that (i) preliminary tests indicated a sharp decrease in the precipitation yield for acid concentrations superior to 1.00 mol.kg$^{-1}$ (> 3.7 wt.% HCl), (ii) the presence of metal ions with conflicting redox potentials such as Fe(II) will impact the Mn precipitation yield and final purity[24-25] and (iii) an excess of $O_3$ could re-dissolve precipitated manganese as permanganate.[24-25]

**Table 1.** Elemental EDS analysis of the precipitates obtained after 480 min ozonation in $H_2O$ and 3.7 wt.% HCl.

| [HCl] (wt.%) | Precipitate composition (wt.%) | | | | |
|---|---|---|---|---|---|
| | **Mn** | **Co** | **Ni** | **Cl** | **Total** |
| **0.0** | 49.6 ± 4.4 | 4.6 ± 0.6 | 8.1 ± 0.9 | 9.2 ± 1.0 | 71.5 |
| **3.7** | 57.5 ± 5.1 | 2.8 ± 0.4 | 3.9 ± 0.5 | 8.2 ± 0.9 | 72.4 |

## Development of a $NiCl_2$-based stimuli responsive ABS

Having demonstrated the selective removal of Mn, the potential of $NiCl_2$ to act as phase former and salting-out agent for the extraction of Co(II) in the $NiCl_2$-[$P_{44414}$]Cl-$H_2O$ ABS is explored. The binodal curves for the system as a function of temperature (25.0 and 50.0 ºC) and HCl concentration (3.7 wt.%) are presented in **Figure 3A** and listed in **Table S1**, with the six water molecules of the $NiCl_2.6H_2O$ salt included in the total water content. At 25 ºC, a significant concentration of $NiCl_2$ is required to induce the ABS formation. To a solution containing 30.0 wt.% [$P_{44414}$]Cl, addition of no less than 12.5 wt.% $NiCl_2$, that is 1.1 mol.kg$^{-1}$ of $NiCl_2$ is required. However, and as expected based on the reported thermomorphic properties of [$P_{44414}$]Cl-based ABS,[16,17] at 50.0 ºC the amount of $NiCl_2$ required to form a biphasic system is reduced by approximately four times for a 30.0 wt.% [$P_{44414}$]Cl solution. Upon addition of 3.7 wt.% HCl to the mixture, the concentration of $NiCl_2$ required to yield a biphasic system is further decreased down to 1.68 wt.%, that is, 0.13 mol.kg$^{-1}$ $NiCl_2$. The acid and temperature responsive nature of the $NiCl_2$-[$P_{44414}$]Cl-$H_2O$ system makes this versatile ABS compatible with a wide range of $NiCl_2$ containing effluents including concentrated NiMH battery leachate solutions.[5]

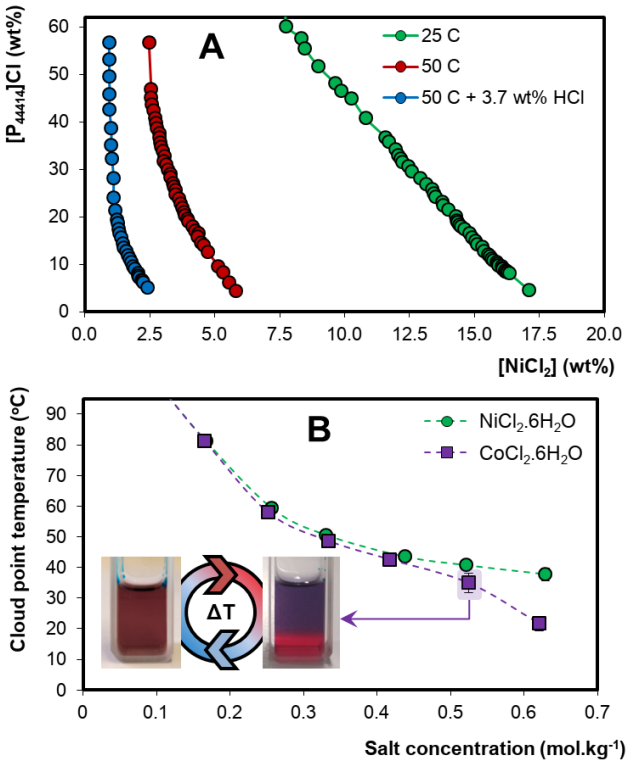


223

224 **Figure 3.** A) Binodal curves of the $NiCl_2$–$[P_{4444}]Cl$–$H_2O$ ABS with temperature and HCl concentration;
225 B) Cloud point curves for $MCl_2$–$[P_{4444}]Cl$–$H_2O$ (M- Ni or Co) as a function of salt concentration
226 ($[P_{44414}]Cl$= 20.0 wt.% or 0.46 mol.kg$^{-1}$). Inset: picture of the highlighted $CoCl_2$–$[P_{4444}]Cl$–$H_2O$ mixture
227 point below (31.0 ºC, left) and above (37.0 ºC, right) its cloud point.

228

229 The study of the $NiCl_2$-$[P_{44414}]Cl$-$H_2O$ ABS is made possible the prevalence of cationic nickel species
230 in both ABS phases as identified by UV-vis, **Figure S6**. In contrast, the equivalent $CoCl_2$-$[P_{44414}]Cl$-
231 $H_2O$ system could not be determined by cloud point titration due to the difference in cobalt speciation
232 between the IL-rich and salt-rich phases as evidenced by the blue and red colour in each respective
233 phase. A visual example of this is presented in the inset picture of **Figure 3B** and the corresponding
234 UV-vis spectra of each phase is available in **Figure S6**. Whilst the red colour is typical of cobalt
235 hexahydrate, the blue coloration is indicative of the anionic tetrahedral chlorocobalt complexes.[7-15] The
236 lower charge density of the $CoCl_3^-$ or $CoCl_4^{2-}$ compared to original chloride anion of $[P_{44414}]Cl$ results
237 in an ion-pair or anion-exchange reactions, Equations (10) to (12), and the formation of a "new" IL with
238 a chlorocobalt anion.

239 $$[P_{44414}]Cl + CoCl_2 \leftrightarrow [P_{44414}][CoCl_3] \quad -(10)$$

240 $$2[P_{44414}]Cl + CoCl_3^- \leftrightarrow [P_{44414}]_2[CoCl_4] + Cl^- \quad -(11)$$

241 $$2[P_{44414}]Cl + CoCl_4^{2-} \leftrightarrow [P_{44414}]_2[CoCl_4] + 2Cl^- \quad -(12)$$

The $CoCl_2$-$[P_{44414}]Cl$-$H_2O$ cannot be considered a typical ABS as the biphasic behaviour is determined by the change in the IL nature brought about by the switch from cationic to anionic cobalt complex. As such an alternative approach was sought to better appreciate how the difference between the $NiCl_2$- and $CoCl_2$-$[P_{44414}]Cl$-$H_2O$ systems can influence Co(II) extraction. A further consideration beyond ABS formation is the minimal salt concentration necessary for Co(II) partition to the IL phase, as the optimal extraction range varies based on the salting-out strength of the chloride source.[13] To this end, the influence of Co(II) and Ni(II) chloride salts concentrations on the cloud point (CP) appearance, corresponding to the first sign of temperature-induced demixing, was assessed (**Figure 3B**). A 20.0 wt.% $[P_{44414}]Cl$ aqueous solution was used as this falls within the micellar regime of the phase diagram and also corresponds to the IL concentration range displaying the largest temperature response in $[P_{44414}]Cl$-based ternary aqueous systems.[17] Due to the similar ionic radii and valency of the hydrated Ni(II) and Co(II) cations, any important deviation between the $NiCl_2$ and $CoCl_2$ phase diagrams can be attributed to speciation effects and the formation of the $[P_{44414}][CoCl_3]$ or $[P_{44414}]_2[CoCl_4]$ IL. From **Figure 3B**, it appears that a threshold concentration of $[MCl_2.6H_2O] \geq 0.50$ mol.kg$^{-1}$ is required as this corresponds to the concentration after which a significant deviation between the $NiCl_2$-$[P_{44414}]Cl$-$H_2O$ and $CoCl_2$-$[P_{44414}]Cl$-$H_2O$ phase diagrams occurs. This deviation is assigned to the increased partition of Co(II) to the IL-rich phase and the resulting formation of the chlorocobalt IL.

Interestingly, in the $CoCl_2$-$[P_{44414}]Cl$-$H_2O$ system under monophasic conditions presented a visible colour change from red to purple as the temperature was raised near the cloud point, suggesting a change in Co(II) speciation prior to phase separation. To better appreciate the possible synergistic effect between temperature, $[P_{44414}]Cl$ phase behaviour and Co(II) speciation, the UV-vis spectra of the $CoCl_2$-$[P_{44414}]Cl$-$H_2O$ mixture point highlighted in **Figure 3B** (0.52 mol.kg$^{-1}$ $CoCl_2.6H_2O$ and 0.46 mol.kg$^{-1}$ $[P_{44414}]Cl$) was monitored as a function of temperature in the monophasic region until close to its CP at 34.9 $^{o}$C. The resulting spectra are presented in **Figure 4A** and present 4 peaks, at 511 nm (peak 1) corresponding to the octahedral Co(II) hexahydrate complex and three peaks at 631 nm (peak 2), 666 nm (peak 3) and 690 nm (peak 4) attributed to the tetrahedral anionic chlorocobalt species.[13] The spectra in **Figure 4A** are standardised according to the $[Co(H_2O)_6]^{2+}$ peak (peak 1) and clearly show the increase with temperature of the characteristic peaks (peaks 2-4) of anionic cobalt species. It is important to stress that the molar extinction coefficient of $[CoCl_4]^{2-}$ is far greater than that of $[Co(H_2O)_6]^{2+}$, implying that anionic chlorocobalt complexes represent but a small fraction of the total Co(II) distribution at this composition. The temperature-dependent octahedral-tetrahedral transition of Co(II) complexes was previously observed in concentrated aqueous solution[27] and in a range of neat ILs.[28-30] However, the thermochromic transition observed in **Figure 4A** over a temperature range of only 24.0 $^{o}$C is notable for its low $[Cl^-]/[Co^{2+}]$ ratio of approximately 3 ($[Cl]^-$ = 1.51 mol.kg$^{-1}$) and its occurrence in a relatively dilute aqueous environment. This is markedly different to that observed in aqueous solutions where Co(II) is predominantly under the form of a positively charged or neutral cobalt(II) complex containing

$H_2O$ and 1 or 2 $Cl^-$ anions for chloride concentrations below 6.0 mol.$L^{-1}$ and only forms anionic chlorocobaltate(II) complexes such as $CoCl_3^-$ and $CoCl_4^{2-}$ when the [Co]/[$H_2O$] ratio is low, typically for HCl ≥ 8 mol.$L^{-1}$.[12,13,31,32]

To assess the relationship between $[CoCl_4]^{2-}$ formation and phase separation, the IL aggregate diameter was estimated by dynamic light scattering (DLS) as a function of temperature (**Figure 4B**). Two aggregation regimes are observable in **Figure 4B**, a micellar domain for T < 31.0 °C (grey shaded area) and a coacervation domain for T ≥ 31.0 °C (orange shaded area) characterised by the formation of large bi-continuous aggregates.[17] The presence of a lower critical solution temperature is an entropically driven phenomenon in which dehydration of the micellar interface is accentuated with temperature increase.[17,33] This interfacial dehydration combined with a greater chloride accumulation compared to the bulk solution could favour the local formation of neutral or anionic chlorocobalt, facilitating their extraction. Relating the micellar aggregate diameter to the corresponding characteristic peak of $[CoCl_4]^{2-}$ for a given temperature below 31.0 °C, inset **Figure 4B**, yields a linear correlation providing some credence to the above assumption. This linear relationship does not apply in the coacervate regime where a break in the slope occurs. Further work is anticipated to confirm this potential synergy between temperature, $[P_{44414}]Cl$ aggregation, Co(II) speciation and their relation to Co(II) extraction.

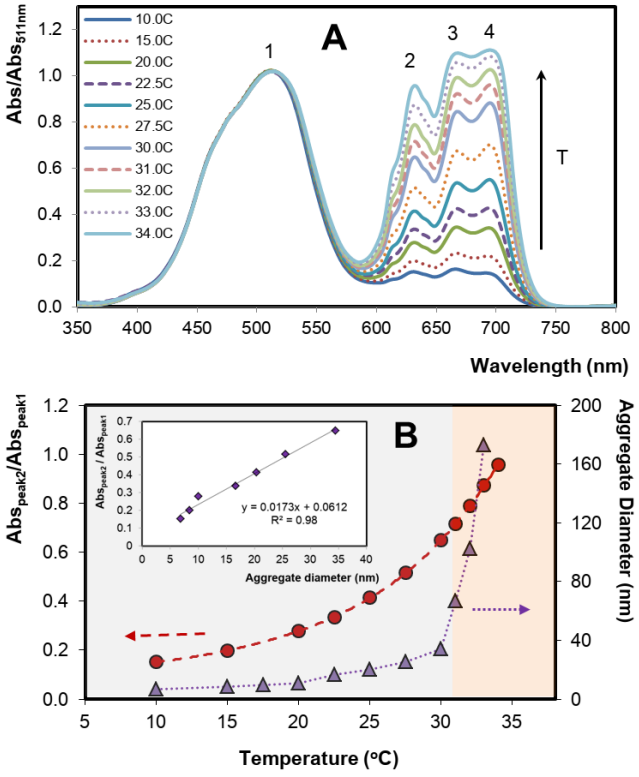


**Figure 4.** A) Temperature dependent UV-vis spectra of the $CoCl_2$-$[P_{44414}]Cl$-$H_2O$ system under monophasic conditions standardised according to the absorbance at 511 nm (peak 1). B) Average

$[P_{44414}]^+$ aggregate size and UV-vis absorbance ratio for peak 2 with temperature, grey and orange shaded area denote the micellar and coacervate zones respectively. Inset: UV-vis absorbance ratio for peak 2 against $[P_{44414}]^+$ aggregate size at a given temperature. A constant system composition of 0.52 mol.kg$^{-1}$ $CoCl_2.6H_2O$ and 0.46 mol.kg$^{-1}$ $[P_{44414}]Cl$ was used.

## Selective cobalt extraction in the $NiCl_2$-based ABS and system regeneration

Based on the results in **Figure 3** and **4**, the separation of Co(II) from concentrated Ni(II) was assessed in three systems: (i) a "chloride deficient" system with $[NiCl_2.6H_2O]$=0.35 mol.kg$^{-1}$, (ii) the same system supplemented with 3.7 wt.% HCl (~ 1.00 mol.kg$^{-1}$) and (iii) a concentrated system with $[NiCl_2.6H_2O]$=1.00 mol.kg$^{-1}$ in the absence of HCl. An IL concentration of 20 wt.% and a separation temperature of 50.0 ºC were used throughout as this expands the operation biphasic region. The separation was estimated as a function of the mole fraction of Co(II) ($\chi_{Co}$) varying between 0.00 and 0.33. As could be expected from the "chloride deficient" system (i), no significant cobalt extraction ($D_{Co} < 0.2$) was observed for all tested Co(II) concentrations and is therefore not further investigated (not shown in **Figure 5**). Adding 3.7 wt.% HCl (system (ii)) leads to quite different results. First , Co(II) partitions preferentially in the IL-rich phase, as indicated by values above 1 for the distribution coefficients of Co(II) observed in **Figure 5A**. In addition, $D_{Co}$ and the Co(II)/Ni(II) separation factor ($\alpha_{Co/Ni}$), increase with the mole fraction of Co. An increase in the ionic strength of the initial solution led to an significant increase of $D_{Co}$ value whilst simultaneously decreasing the distribution of Ni(II) to the IL phase. This results in an increase in $\alpha_{Co/Ni}$ from 2.4 for $\chi_{Co}$ = 0.05 to 14.9 for $\chi_{Co}$ = 0.33. A more detailed analysis of Co(II) extraction in this system as a function of HCl concentration was previously studied and is not addressed in this work.[11,14] Rather counterintuitively, $\alpha_{Co/Ni}$ is greatly improved when the Ni(II) concentration is raised to $[NiCl_2.6H_2O]$= 1.00 mol.kg$^{-1}$, system (iii) presented in **Figure 5B**, reaching a maximum separation value of 484 for $\chi_{Co}$ = 0.20.

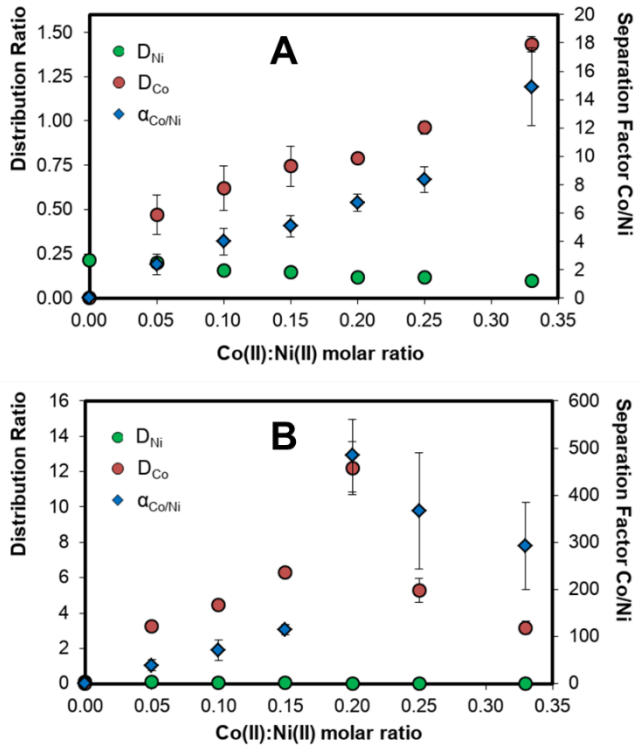


**Figure 5.** Co(II) and Ni(II) distribution and Co/Ni separation for $[P_{44414}]Cl$= 20.0 wt.% at varying Co molar fractions for A) $[NiCl_2.6H_2O]$=0.35 mol.kg$^{-1}$ with 3.7 wt.% HCl and B) $[NiCl_2.6H_2O]$=1.00 mol.kg$^{-1}$ (data available in **Table S2 & S3** of the SI). Results are the average of three independent measurements.

However, it must be considered that the total chloride concentration and the ionic strength (*I*) in system (iii) ($[Cl]^- \approx 2.46$ mol.kg$^{-1}$ and $I \approx 5.10$ mol.kg$^{-1}$) are both greater than in system (ii) ($[Cl]^- \approx 2.16$ mol.kg$^{-1}$ and $I \approx 3.20$ mol.kg$^{-1}$) without accounting for the additional $CoCl_2$ concentration. This in turn influences the activity of each species in solution and facilitates the formation of anionic cobalt complexes. As no additional chloride source is present in solution beyond $[P_{44414}]Cl$, $CoCl_2$ and $NiCl_2$ in system (iii), to satisfy electroneutrality Co(II) can only partition to the IL phase via an ion-pair mechanism. Assuming $[P_{44414}]_2[CoCl_4]$ as the predominant complex in the IL phase after extraction and given an IL concentration of $[P_{44414}]Cl$ =0.46 mol.kg$^{-1}$ (20.0 wt.%), the decrease in $D_{Co}$ when the concentration of Co(II) is above 0.20 mol.kg$^{-1}$ ($\chi_{Co}$ >0.20 in **Figure 5B**) is attributed to the saturation of the IL phase. A second possible explanation is the reported decrease in Co(II) extraction when present as $CoCl_4^{2-}$ compared to $CoCl_3^-$ due to its greater relative charge density.[7-11,13-15] The increase in ionic strength with increasing $\chi_{Co}$ in system (iii) can change the predominant Co(II) complex, $I \approx 5.10$ mol.kg$^{-1}$ for $\chi_{Co}$=0.00 and $I \approx 7.20$ mol.kg$^{-1}$ for $\chi_{Co}$=0.33, with this change reflected in the distribution ratio. Separation results in **Figure 5A-B** suggest that under appropriate conditions, namely a high $NiCl_2$ concentration and a $[P_{44414}]Cl$ to Co molar ratio near to saturation (2:1), Co(II) can be directly recovered

from $NiCl_2$ solutions with moderate distribution but high purity comparable to that obtained in the presence of an additional chloride source.[7,11,14,15] At the optimal extraction condition in **Figure 5B**, no peaks characteristic of the $[P_{44414}]^+$ cation could be detected by $^1$H-NMR in the salt-rich phase (detection limit - 5 mol.%), indicating negligible loss of the IL.

As the system is fully aqueous a larger number of cobalt recovery routes are available compared to hydrophobic IL systems. We previously showed that cobalt could be electrodeposited from the studied system.[11] Here, a one step process for the simultaneous precipitation of Co(II) and recovery of the IL is proposed based on a $Na_2CO_3$-$[P_{44414}]Cl$-$H_2O$ ABS at 25.0 $^oC$ (**Figure S7**). $Na_2CO_3$ was selected as precipitant as the greater ionicity of the carbonate anion compared to chloride should minimise anion-exchange whilst promoting the IL phase separation and recovery. The final quality of the precipitate was evaluated based on the predominant cobalt complex in solution, anionic *vs* hexahydrate, prior to $Na_2CO_3$ addition. Following extraction in system (iii) at $\chi_{Co}$ = 0.20 and isolation of the IL-rich upper phase (Co rich), the latter was diluted either 3 times or 8 times resulting in a blue and red solution respectively, assigned to the change in cobalt speciation as previously discussed. After addition of a stoichiometric quantity of $Na_2CO_3$ to Co(II), the precipitate was isolated by centrifugation and rinsed with deionized water and ethanol. The FTIR spectra of the resulting precipitates are presented in **Figure 6A**. The bands characteristic of alkyl moieties highlighted in **Figure 6A** clearly indicate the co-precipitation of the IL with Co(II) when Co(II) is present in an anionic form (x3 diluted), bands which persist even after rinsing. The absence of these vibrational modes in the precipitate obtained after 8x dilution of the IL-phase suggests that conversion of Co(II) to its cationic hexahydrated form is essential to minimise IL loss and ensure the precipitate purity. SEM-EDS analysis of the purple precipitate obtained after eight-fold dilution of the IL phase is presented in **Figure S8** and **Figure 6B**, confirming the absence of both IL and Ni(II) in the final precipitate and the primary presence of cobalt as $CoCO_3$.

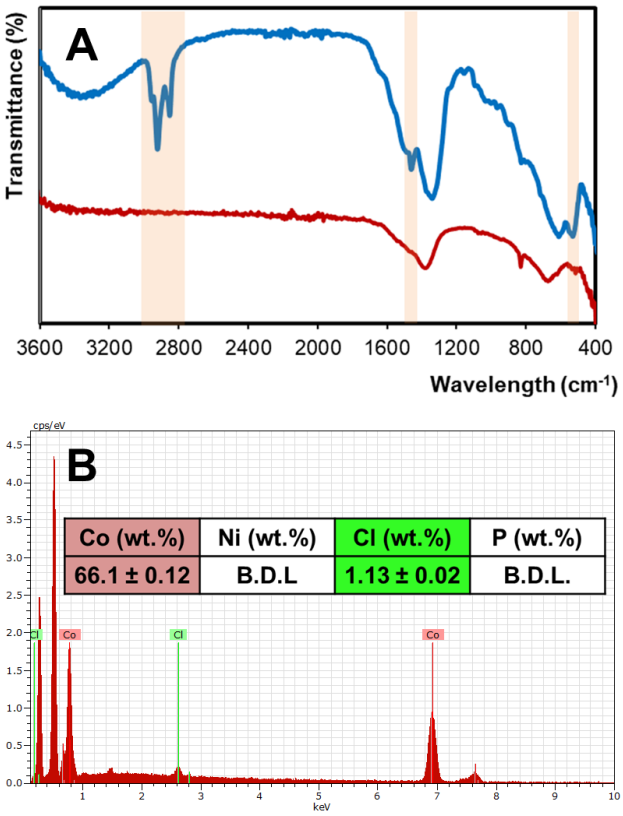


**Figure 6.** FTIR spectra of the precipitate obtained after 3x (blue) and 8x (red) dilution of isolated IL phase and addition of $Na_2CO_3$. B) Energy dispersive X-ray analysis of the recovered precipitate from the 8x diluted IL phase (green label – chloride, red label – cobalt; BDL – Below detection limit). Extraction conditions prior to precipitation - $\chi_{Co}$ = 0.20 and $[NiCl_2.6H_2O]$=1.00 mol.kg$^{-1}$.

After the precipitate recovery, additional $Na_2CO_3$ was added to the IL solution to yield a final concentration of $[Na_2CO_3]$ = 10.0 wt.% (see **Figure S7**) resulting in phase separation of the system into and IL-rich phase and carbonate-rich phase. The isolated IL-rich phase was characterised by $^{1}$H-, $^{12}$C- and $^{31}$P-NMR (**Figure S9**) and FTIR (**Figure 7**). Although phosphonium ILs can decompose to yield a tertiary phosphine oxide and alkane under alkaline conditions,[34] no changes in the $^{31}$P-NMR spectra was observed relative to the starting IL. Additionally, NMR and FTIR confirm the absence of carbonate anions in the recovered phase, allowing the IL to be reused, whilst $^{1}$H-NMR of the salt-rich phase could not detect the $[P_{44414}]^+$ cation. To the best of our knowledge, this represents the first example of an ABS for simultaneous metal recovery and IL regeneration, representing an integrated approached to metal processing.

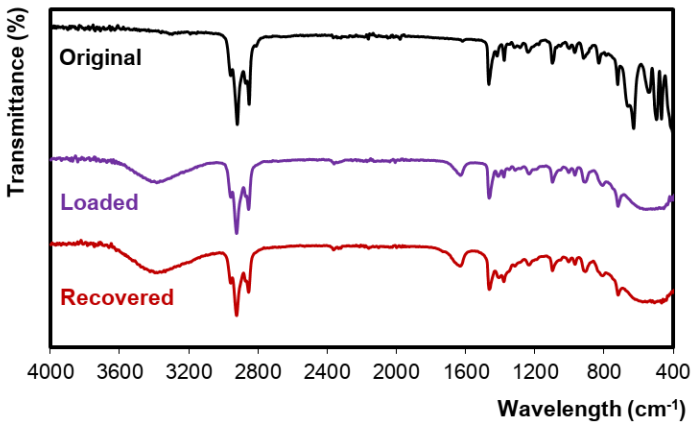


385

386 **Figure 7.** FTIR spectra of the original [$P_{44414}$]Cl, after extraction of Co(II) and after Co(II) precipitation
387 and IL recovery.

388

389 Co(II) could be selectively recovered from large concentrations of Ni(II) impurities in a stimuli
390 responsive ABS with no additional salt addition by manipulation of temperature, HCl concentration and
391 ionic strength, providing a closed loop process for Co(II) recovery with minimal reagent consumption
392 and recovery of the IL phase. Further work is necessary to extend the proposed process for systems
393 presenting an Ni(II):Co(II) ratio equal to or lower than 1 typical of lithium-ion battery composition.[1]
394 The metal concentrations studied in this work are characterised by high Ni(II):Co(II) ratios as an excess
395 of Ni(II) is required to induce the biphasic system and salt-out the anionic chlorocobalt complexes as
396 shown in **Figure 5**. Whilst lower Ni(II):Co(II) ratios are unlikely to significantly affect the purity of the
397 recovered Co(II) due to the inability of Ni(II) to form the required anionic complexes required for
398 extraction, optimisation is required to minimise a decrease in the distribution of Co(II) to the IL phase.
399 Comparison with other reported ABS in **Table 2** present comparable or higher Co(II)/Ni(II) separation
400 factors due to their greater reported $D_{Co}$ but at the expense of increased separation complexity.
401 Extraction in polymer-based ABS requires the decrease of the hydration entropy of the metal complex
402 either through the addition of ligands such as thiocyanate anions such as to form anionic metal
403 complexes or through complexation with a hydrophobic ligand.[35] Unlike extraction in the proposed
404 system that is robust to pH variations and improves with HCl concentration, separation in the presence
405 of an acidic extractant depends both on the choice of extractant as well as optimisation of pH, implying
406 increased process control and monitoring.

407

408 **Table 2.** Comparison various ABS performance on the extraction and separation of Co(II) from Ni(II)
409 (1N2N – 1-nitroso 2-naphthol; PAN – 1-(2-pyridylazo)-2-naphthol).

| System | Extractant | $D_{Co}$ | $\alpha_{Co/Ni}$ | Ref |
|---|---|---|---|---|

| | | | | |
|---|---|---|---|---|
| $[P_{44414}]Cl – NiCl_2 – H_2O$ | – | 14.9 | 484 | This work |
| $[P_{44414}]Cl – NaCl – H_2O$ | – | 100 | 500 | 15 |
| $PEO1500 – (NH_4)_2SO_4 – H_2O$ | KSCN | 499 | > 1000 | 36 |
| $L64 – Na_2SO_4 – H_2O$ | 1N2N | 122 | > 1000 | 37 |
| $PEG\text{-}2000 – (NH_4)_2SO_4 – H_2O$ | PAN | 10.0 | < 10 | 38 |

The influence of metal impurities on the efficiency of Mn(II) precipitation and Co(II) extraction selectivity is required prior to the application of real battery leachates. The presence of metal ions with conflicting redox potentials could negatively impact the Mn(II) precipitation yield and final purity. Potential interferences include Fe(II)/Fe(III) or the redox couple Ce(III)/$CeO_2$ under neutral pH conditions. Although Fe is not included in the anode/cathode composition of NiMH batteries, it is frequently co-leached due to its presence in the battery casing and anode plate.[5] Whilst the presence of Fe(II) would hinder the conversion of $MnO_2$,[24] iron is typically present as Fe(III) in the leach solution and should therefore present minimal interference.[5] The Pourbaix diagram of the Ce(III) aqueous system shows that under acidic condition (pH < 1) the redox potential of the Ce(III)/Ce(IV) couple is of $E^0$= 1.743 V, largely above that of Mn(II)/Mn(IV).[39] Under neutral pH, the redox couple of Ce(III)/$CeO_2$ could potentially interfere although more work is required to assess its influence. Metal extraction in $[P_{44414}]Cl$ is dominated by ion-pair or anion-exchange mechanisms, which depends on the capacity of a metal ion to form neutral or anionic complexes with a given ligand, in this case chloride. From the metals present in NiMH batteries, rare earth elements are not extracted in these chloride systems and could increase the partition of Co(II) through an increase in the solution ionic strength.[9] The presence of Zn(II) and Fe(III) however would however conflict with the extraction of Co(II) as these are extracted at lower chloride concentrations and diminish both the Co(II) distribution factor and selectivity.[13]

## Conclusions

A fully aqueous process for the problematic separation of Mn(II) and Co(II) from concentrated Ni(II) solutions of relevance to waste battery recycling is disclosed. In a first instance, Mn(II) was selectively precipitated by oxidation under the form of $MnO_2$ using $O_3$ in presence of excess impurities and enriched 16.6 times in the precipitate compared to its original solution concentration. Following Mn(II) removal, the $NiCl_2$-$[P_{44414}]Cl$-$H_2O$ ABS was investigated for the direct recovery of Co(II) in the absence of an external chloride source. The versatility of aqueous $[P_{44414}]Cl$ solutions and its phase behaviour allows for the thermochromic transition of cobalt speciation and its efficient recovery from concentrated Ni(II) solutions. The metal composition studied are in line with that found in NiMH battery leachates, with future work planned to extend the separation to compositions corresponding to those found in

lithium-ion batteries. Finally, high purity Co(II) was recovered by $Na_2CO_3$ addition and subsequent precipitation and the IL was regenerated, allowing for a closed-loop process with no consumption of reagents except $Na_2CO_3$.

## Supporting Information

The Supporting Information is available free of charge and includes the Materials and Methods used; Calibration procedure for the ozone generator; Determination of $MCl_2$-[$P_{44414}$]Cl-$H_2O$ phase diagrams and the experimental binodal data; Evolution of the cobalt and nickel concentration with time during the continued ozonation of manganese; SEM-EDS characterisation of the recovered precipitates; Binodal curve of the $Na_2CO_3$–[$P_{4444}$]Cl–$H_2O$ ABS at 25.0 ºC; NMR spectra of virgin and recovered [$P_{44414}$]Cl; Cobalt and nickel distribution coefficients as a function of the cobalt:nickel molar ratio.

## Acknowledgements

This work was developed within the scope of the project CICECO-Aveiro Institute of Materials, UIDB/50011/2020 & UIDP/50011/2020, financed by national funds through the Foundation for Science and Technology/MCTES. This work was part of BATRE-ARES Project (ERA-MIN/0001/2015) funded by ADEME and FCT. H. Passos acknowledges FCT – Fundação para a Ciência e a Tecnologia, I.P., under the Scientific Employment Stimulus - Individual Call - CEECIND/00831/2017 - under the CEEC Individual 2017. M.C. Neves acknowledges FCT, I.P. for the research contract CEECIND/00383/2017 under the Scientific Employment Stimulus - Individual Call. M.G. would like to acknowledge labex CEMAM and EIT InnoEnergy H2020 for financial support.

## References

[1] Fan, E.; Li, L.; Wang, Z.; Lin, J.; Huang, Y.; Yao, Y.; Chen, R.; Wu, F. Sustainable Recycling Technology for Li-Ion Batteries and Beyond: Challenges and Future Prospects. *Chem. Rev.* **2020**, DOI: 10.1021/acs.chemrev.9b00535.

[2] European Commission, Batteries and Accumulators, **2020** [accessed: 10/02/2020].

[3] Harper, G.; Sommerville, R.; Kendrick, E.; Driscoll, L.; Slater, P.; Stolkin, R.;Walton, A.; Christensen, P.; Heidrich, O.; Lambert, S.; Abbott, A.; Ryder, K.; Gaines, L.; Anderson, P. Recycling lithium-ion batteries from electric vehicles. *Nature*, **2019**, 575**,** 75–86, DOI: 10.1038/s41586-019-1682-5.

[4] Innocenzi, V.; Ippolito, N.M.; De Michelis, I.; Prisciandaro, M.; Medici, F.; Vegliò, F. A review of the processes and lab-scale techniques for the treatment of spent rechargeable NiMH batteries. *J. Power Sources*, **2017**, 362, 202-218, DOI: 10.1016/j.jpowsour.2017.07.034.

[5] Larsson, K.; Ekberg, C.; Ødegaard-Jensen, A. Dissolution and characterization of HEV NiMH batteries. *Waste Manage.*, **2013**, 33, 689-698, DOI: 10.1016/j.wasman.2012.06.001.

[6] Schaeffer, N.; Passos, H.; Billard, I.; Papaiconomou, N.; Coutinho, J.A.P. Recovery of Metals from Waste Electrical and Electronic Equipment (WEEE) Using Unconventional Solvents Based on Ionic Liquid. *Crit. Rev. Env. Sci. Tec.*, **2018**, 48, 859-922, DOI : 10.1080/10643389.2018.1477417.

[7] Wellens, S.; Thijs, B.; Binnemans, K. An environmentally friendlier approach to hydrometallurgy: highly selective separation of cobalt from nickel by solvent extraction with undiluted phosphonium ionic liquids. *Green Chem.*, **2012**, 14, 1657-1665, DOI: 10.1039/C2GC35246J.

[8] Wellens, S.; Goovaerts, R.; Möller, C.; Luyten, J.; Thijs, B.; Binnemans, K. A continuous ionic liquid extraction process for the separation of cobalt from nickel. *Green Chem.*, **2013**, 15, 3160-3164, DOI: 10.1039/C3GC41519H.

[9] Larsson, K.; Binnemans, K. Selective extraction of metals using ionic liquids for nickel metal hydride battery recycling. *Green Chem.*, **2014**, 16, 4595-4603, DOI: 10.1039/C3GC41930D.

[10] Larsson, K.; Binnemans, K. Metal Recovery from Nickel Metal Hydride Batteries Using Cyanex 923 in Tricaprylylmethylammonium Nitrate from Chloride Aqueous Media. *J. Sustain. Metall.*, **2015**, 1, 161–167

[11] Schaeffer, N.; Gras, M.; Passos, H.; Mogilireddy, V.; Mendonça, C.M.N.; Pereira, E.; Chainet, E.; Billard, I.; Coutinho, J.A.P.; Papaiconomou, N. Synergistic Aqueous Biphasic Systems: A New Paradigm for the "One-Pot" Hydrometallurgical Recovery of Critical Metals. *ACS Sustain. Chem. Eng.*, **2019**, 7, 1769-1777, DOI: 10.1021/acssuschemeng.8b05754.

[12] Högfeldt, E., IUPAC Stability constants of metal-ion Complexes Part A: Inorganic ligands; IUPAC; Pergamon Press, **1982**.

[13] Lommelen, R.; Vander Hoogerstraete, T.; Onghena, B.; Billard, I.; Binnemans, K. Model for Metal Extraction from Chloride Media with Basic Extractants: A Coordination Chemistry Approach. *Inorg. Chem.* **2019**, 58, 12289-12301, DOI: 10.1021/acs.inorgchem.9b01782.

[14] Gras, M.; Papaiconomou, N.; Schaeffer, N.; Chainet, E.; Tedjar, F.; Coutinho, J.A.P.; Billard, I. Ionic-Liquid-Based Acidic Aqueous Biphasic Systems for Simultaneous Leaching and Extraction of Metallic Ions. *Angew. Chem. Int.*, **2018**, 57, 1563-1566, DOI: 10.1002/anie.201711068.

[15] Onghena, B.; Opsomer, T.; Binnemans, K. Separation of cobalt and nickel using a thermomorphic ionic-liquid-based aqueous biphasic system. *Chem. Commun*., 2015, 51, 15932-15935, DOI: 10.1039/C5CC06595J.

[16] Schaeffer, N.; Passos, H.; Gras, M.; Mogilireddy, V.; Leal, J.P.; Perez-Sanchez, G.; Gomes, J.R.B.; Billard, I.; Papaiconomou, N.; Coutinho, J.A.P. Mechanism of Ionic Liquid-Based Acidic Aqueous Biphasic Systems Formation. *Phys. Chem. Chem. Phys.*, **2018**, 20, 9838-9846, DOI: 10.1039/C8CP00937F.

[17] Schaeffer, N.; Pérez-Sánchez, G.; Passos, H.; Gomes, J.R.B.; Papaiconomou, N.; Coutinho, J.A.P. Mechanisms of Phase Separation in Temperature-Responsive Acidic Aqueous Biphasic Systems. *Phys. Chem. Chem. Phys.*, **2019**, 21, 7462 – 7473, DOI: 10.1039/C8CP07750A.

[18] Neves, C.M.S.S.; Ventura, S.P.M.; Freire, M.G.; Marrucho, I.M.; Coutinho, J.A.P. Evaluation of Cation Influence on the Formation and Extraction Capability of Ionic-Liquid-Based Aqueous Biphasic Systems. *J. Phys. Chem. B*, **2009**, 113, 5194−5199, DOI: 10.1021/jp900293v.

[19] Ji, J.; Cooper, W.C. Nickel speciation in aqueous chloride solutions. *Electrochim. Acta*, 1996, 41, 1549-1560, DOI: 10.1016/0013-4686(95)00407-6.

[20] Tian, Y.; Etschmann, B.; Mei, Y.; Grundler, P.V.; Testemale, D.; Hazemann, J.-L.; Elliott, P.; Ngothai, Y.; Brugger, J. Speciation and thermodynamic properties of manganese(II) chloride complexes in hydrothermal fluids: In situ XAS study. *Geochim. Cosmochim. Acta*, **2014**, 129, 77-95, DOI: 10.1016/j.gca.2013.12.003.

[21] Zheng, X.; Zhu, Z.; Lin, X.; Zhang, Li; He, Y.; Cao, H.; Sun, Z. A Mini-Review on Metal Recycling from Spent Lithium Ion Batteries. *Engineering*, **2018**, 4, 361-370, DOI: 10.1016/j.eng.2018.05.018.

[22] Swain, H.A.; Lee, C.; Rozelle, R.B. Determination of the solubility of manganese hydroxide and manganese dioxide at 25.deg. by atomic absorption spectrometry. *Anal. Chem*. **1975**, 47, 7, 1135-1137, DOI: 10.1021/ac60357a069.

[23] Yamaguchi, K.S.; Sawyer, D.T. The Redox Chemistry of Manganese(III) and -(IV) Complexes. *Isr. J. Chem.*, **1985**, 25, 164-176, DOI: 10.1002/ijch.198500026.

[24] Reckhow D.A.; Knocke, W.R.; Kearney, M.J.; Parks, C.A. Oxidation Of Iron And Manganese By Ozone. *Ozone Sci. Eng.*, **1991**, 13, 675-695, DOI: 10.1080/01919512.1991.10555708.

[25] Tobiason, J.E.; Bazilio, A.; Goodwill, J.; Mai, X.; Nguyen, C. Manganese Removal from Drinking Water Sources. *Curr. Pollut. Rep.*, 2016, 2, 168-177, DOI: 10.1007/s40726-016-0036-2.

[26] Johnson, D.C.; Napp, D.T.; Bruckenstein, S. Electrochemical reduction of ozone in acidic media. *Anal. Chem*., **1968**, 40, 482–488, DOI: 10.1021/ac60259a031.

[27] Ma, H.; Wan, C.; Zewail, A.H. Dynamics of ligand substitution in labile cobalt complexes resolved by ultrafast T-jump. *PNAS*, **2008**,105, 12754–12757, DOI: 10.1073/pnas.0806869105.

[28] McCourt, E.; Wojnarowska, Z.; Jacquemin, J.; Nockemann, P.; Manyar, H.G.; Hawelek, L.; Paluch, M. Temperature- and Pressure-Induced Structural Changes of Cobalt(II) in a Phosphonium-Based Ionic Liquid. *J. Phys. Chem. C*, **2016**, 120, 10156-10161, DOI: 10.1021/acs.jpcc.6b01325.

[29] May, B.; Hönle, M.; Heller, B.; Greco, F.; Bhuin, R.; Steinrück, H.P.; Maier, F. Surface-Induced Changes in the Thermochromic Transformation of an Ionic Liquid Cobalt Thiocyanate Complex. *J. Phys. Chem. Lett*., **2017**, 8, 1137-1141, DOI: 10.1021/acs.jpclett.7b00142.

[30] Billeci, F.; Nimal Gunaratne, H.Q.; D'Anna, F.; Morgan, G.G.; Seddon, K.R.; Plechkova, N.V. A magnetic self-contained thermochromic system with convenient temperature range. *Green Chem*., **2019**, 21, 1412-1416, DOI: 10.1039/C8GC03906B.

[31] Ballhausen, C.; Jørgensen, C.K. Studies of absorption spectra, the spectra of cobalt (II) complexes. *Acta Chem. Scand.,* **1955**, 9, 397–404, DOI: 10.3891/acta.chem.scand.09-0397.

[32] Bjerrum, J.; Halonin, A.S.; Skilsted, L.H. Studies on cobalt (II) halide complex formation. A spectrophotometric study of the chlorocobalt (II) complexes in strong aqueous chloride solution. *Acta Chem. Scand.,* **1975**, 29, 326–332, DOI: 10.3891/acta.chem.scand.29a-0326.

[33] Naqvi, A.Z., Kabir-Ud-Din. Clouding Phenomenon in Amphiphilic Systems: A Review of Five Decades. *Colloids Surf., B,* **2018**, 165, 325–344, DOI: 10.1016/j.colsurfb.2018.01.060.

[34] Bradaric, C.J.; Downard, A.; Kennedy, C.; Robertson, A.J.; Zhou, Y. Industrial preparation of phosphonium ionic liquids. *Green Chem.*, **2003**, 5, 143-152, DOI: 10.1039/B209734F.

[35] Karmakar, R.; Sen, K. Aqueous biphasic extraction of metal ions: An alternative technology for metal regeneration. *J. Mol. Liq.*, **2019**, 273, 231-247, DOI: 10.1016/j.molliq.2018.10.036.

[36] da Rocha Patrício , P.; Cabral, M.C.; da Silva, L.H.M.; da Silva, M.C.H. Application of Aqueous Two-Phase Systems for the Development of a New Method of cobalt(II), iron(III) and nickel(II) Extraction: A Green Chemistry Approach. *J Hazard Mater.*, **2011**, 193, 311-318, DOI: 10.1016/j.jhazmat.2011.07.062.

[37] Valadares, A.; Valadares, C.F.; de Lemos, L.R.; Mageste, A.B.; Rodrigues, G.D. Separation of cobalt and nickel in leach solutions of spent nickel-metal hydride batteries using aqueous two-phase systems (ATPS). *Hydrometallurgy*, **2018**, 181, 180-188, DOI: 10.1016/j.hydromet.2018.09.006.

564 [38] Visser, A.E.; Griffin, S.T.; Hartman, D.H.; Rogers, R.D. Naphthol- And Resorcinol-Based Azo
565 Dyes as Metal Ion Complexants in Aqueous Biphasic Systems. *J. Chromatogr. B.*, **2000**, 743, 107-114,
566 DOI: 10.1016/S0378-4347(00)00176-6.

567 [39] Yu, P.; Hayes, S.A.; O'Keefe, T.J.; O'Keefe, M.J.; Stoffer, J.O. The Phase Stability of Cerium
568 Species in Aqueous Systems: II. The Systems. Equilibrium Considerations and Pourbaix Diagram
569 Calculations. *J. Electrochem. Soc*., **2005**, 153, C74-C79, DOI: 10.1149/1.2130572.

570

571

572

573

574

575

576

## Table of Content Graphic

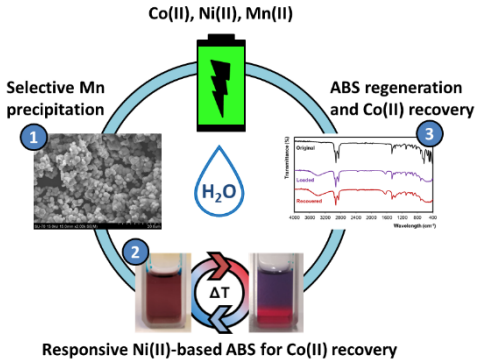


## Synopsis

Development of a fully aqueous process for the separation of Mn(II)/Co(II)/Ni(II) with minimal reagent consumption.